Structure, Dielectric and Impedance Studies of Li Doped $(K_{0.5}Na_{0.5})NbO_3$ Ceramics

Muhammad Asif Rafiq[a], *Muhammad Nadeem Rafiq*[b,c], *Furqan Ahmed*[a], *Liaqat Ali*[a], *Muhammad Yousaf Anwar*[a]

asifrafiq@uet.edu.pk, nadeemrafiq@ciitlahore.edu.pk, furqan.ahmed@uet.edu.pk, liaqat_kasuri@uet.edu.pk, myanwar@uet.edu.pk

[a]Department of Metallurgical and Materials Engineering, University of Engineering and Technology, Lahore, Pakistan

[b]Electrical & Computer Engineering Department, NDSU, Fargo, USA

[c]Department of Electrical Engineering, COMSATS Institute of Information Technology, Lahore, Pakistan

Abstract

Polycrystalline, lead free $(K_{0.5}Na_{0.5})NbO_3$ and $(K_{0.5}Na0.5)_{0.49}Li_{0.02}NbO_3$ ceramics were synthesized using solid-state reaction method. X-ray diffraction studies confirmed the formation of mono-phasic ceramics. During dielectric studies some anomalies were observed around temperatures 155 ºC and 439 ºC for $(K_{0.5}Na0.5)_{0.49}Li_{0.02}NbO_3$. Complex impedance spectroscopy (CIS) technique was used to investigate the bulk (grain interior) and grain boundary contributions to the impedance as a function of temperature and frequency. CIS studies revealed that the electrical relaxation process was temperature dependent and non-Debye type. AC conductivity studies revealed that conductivity was mainly due to the ionized oxygen vacancies in $(K_{0.5}Na0.5)_{0.49}Li_{0.02}NbO_3$ ceramics.

Key words: Polycrystalline, lead free, mono-phasic, non-Debye, impedance spectroscopy.

1. Introduction

In the modern sensor based society, functional ceramics plays a vital role. Their applications include piezoelectric fuel injection, piezoelectric motors, piezoelectric printing machines, piezoelectrically controlled thread guides, micro positioning systems, piezoelectric sensors among many others. Most successful piezoelectrics, from the application point of view, belongs to the solid solution of $PbZr_xTi_{1-x}O_3$ (PZT) system [1]. The high electromechanical properties in PZT were found close to the morphotrophic phase boundary (MPB) with a composition of about x = 0.5. The major drawback of PZT is the high contents of lead (60 wt %), which is toxic in nature and harmful for humans and environment. With the current most restrict environment directives; there is a strong need to the search for lead free alternatives to replace PZT.

$K_{0.5}N_{0.5}NbO_3$ (KNN) is currently being considered one of the most promising lead free composition to replace PZT. KNN is a ferroelectric perovskite with a relatively high Curie point (T_c) of ~ 420 °C [2]. $KNbO_3$ and $NaNbO_3$ form a solid solution of $K_{1-x}Na_xNbO_3$ (KNN) over the entire range of $0 < x < 1$. So far, maximum of the properties were reported for the composition with $x = 0.5$ [3]. $K_{0.5}N_{0.5}NbO_3$ (KNN) presents two phase changes during cooling/heating: one at about 415 ºC, from cubic (C) to ferroelectric tetragonal (T) and another one at 210 ºC, from T to ferroelectric orthorhombic (O) / monoclinic (M) phase [3-7]. In 2004, Saito et al. [8] reported that, that KNN properties can be improved by multiple doping of Li^{1+}, Ta^{5+} and Sb^{5}). Later, following the work of Saito et al., many researchers reported the significant improved room temperature electromechanical properties due to Li^{1+} , Ta^{5+} , and/or Sb^{5+} substitutions [9-15].

In polycrystalline ceramics, defects and inhomogeneities such as grain boundaries (intrinsic defects), point defects etc. are inevitable. Major defects associated with KNN, which can influence its conductivity are oxygen vacancies, alkaline vacancies and space charges. These defects can interact with domain walls, which may strongly affect the electrical properties of these ceramics [16, 17]. Indeed, understanding the nature of these defects and charge transport is fundamental to control the electrical performance of KNN ceramics.

Complex impedance spectroscopy (CIS) is a powerful non-destructive method, widely used to characterize electrical materials [18, 19]. IS is a very useful technique to analyze the electrical response of materials, and to separate bulk, grain boundary and electrode / ceramic interface contributions from the overall electrical response. Furthermore, it can be used to identify conduction mechanisms and even to characterize ferroelectric phase transitions [20-22].

The display of impedance data in the complex plane plot appears in the form of a succession of semicircles due to relaxation phenomena with different time constants of grain (bulk), grain boundary, and interface/polarization in a polycrystalline material. On this basis, it is easy to separate the contribution of various components in the material from overall electrical properties.

In the present work, a detailed and comparative investigation of the conduction behaviour, impedance, electric modulus and transport properties of polycrystalline KNN and Li doped KNN ceramics were studied. Li is selected to substitute for the A-site. To the best of our knowledge, detailed impedance spectroscopy studies in Li-doped KNN bulk ceramics is still rare. Hence, the associated activation energies for conduction is carried out to reveal the nature of defects. The insights gained with this analysis might allow designing KNN based materials with optimized performance for selective uses.

2. Experimental

High purity chemical reagents of K_2CO_3 (Merck, ≥99%), Na_2CO_3 (Chempur, ≥ 99.5%), Nb_2O_5 (Chempur, 99.9%), and Li_2CO_2 (Merck, 99%) were used as starting reagents to prepare undoped $K_{0.5}Na_{0.5}NbO_3$; (KNN) and Li doped KNN; $(K_{0.5}Na_{0.5})_{0.98}Li_{0.02}NbO_3$; (KNNL). Sample powders were first synthesized by a conventional solid-state reaction. The starting reagents in the proper stoichiometric ratio were mixed by ball-milling in teflon pots with ethanol as a solvent for 5 h using zirconia balls. Before weighing and mixing, reagents were dried at 230 °C for 5 h. Then the mixture was calcined at 800 °C for 2 h to obtain the perovskite phase. After calcination, powders were milled again for 5 h and dried. Then ceramics were pressed by uniaxial pressure at 170 MPa followed by a cold isostatic pressing at 200 MPa. Sintering was carried out at 1100 ºC for 2 h.
The crystalline phases were evaluated by X-ray diffraction (XRD, Rigaku, D/Max-B, Cu-K_α radiation) at room temperature in 20° to 60°, 2θ range with a step length of 0.02°. Prior to electrical measurements, the pellets were coated with silver paint on either side and fired at 550 °C for an hour. The dielectric and impedance studies were performed using HP4184A impedance analyzer.

3. Results and Discussion

Figure 1 presents the XRD patterns of undoped KNN and Li doped KNN ceramics sintered at 1100 °C for 2 h. Undoped KNN and Li doped ceramics showed mono-phasic perovskite structure having orthorhombic symmetry with slight monoclinic distortion and no additional second phases have been detected within the resolution limit of the equipment. The lattice parameters of undoped KNN ceramic with a = 3.999 Å, b = 3.948 Å, c = 3.998 Å, and β= 90.21º match closely to the values already reported in the literature [6, 23]. Whereas, with the addition of Li, lattice parameters of a = 4.002 Å, b = 3.946 Å, c = 3.982 Å, and β= 90.44º were obtained for monoclinic (Pm space group) similar to the previously reported values of Li doped KNN ceramics [7, 24].

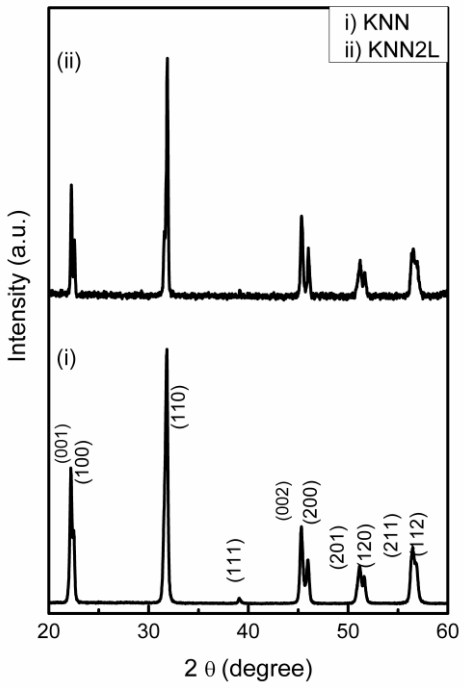

Figure 1: XRD patterns of undoped KNN and Li doped KNN ceramics.

Temperature dependence of the dielectric permittivity and tangent loss (dielectric loss) of the samples were measured at 10 kHz , Figure 2. It wass found that the value of the dielectric constant was not significantly affected by Li substitution at the A-site. Two anomalies (peaks) were observed around 200 ºC and 400 ºC in both cases. Two peaks in the dielectric permittivity can be correlated to the phase transition from cubic to tetragonal ($C \rightarrow T$; T_C) and tetragonal to monoclinic ($T \rightarrow M$) upon cooling. The $T_{O\text{-}T}$ phase transition temperature for KNN was found to be 213 ℃, while T_c was measured as 417 °C, which are very close to the reported values in the literature values [25, 26]. T_C increased to 439 ºC and $T_{O\text{-}T}$ decreased for KNNL 155 ºC which are close to the values reported in the literature [27]. In both cases, at higher temperatures, a strong increase of the dielectric constant was observed which could be related to thermally-induced enhancement of the hopping conduction and/or dipole orientation thereby enhancing the dielectric permittivity. Furthermore, both ceramics showed low dielectric losses and values remained low upto 300 ºC and increase was observed afterwards, which might be related to movement of oxygen vacancies.

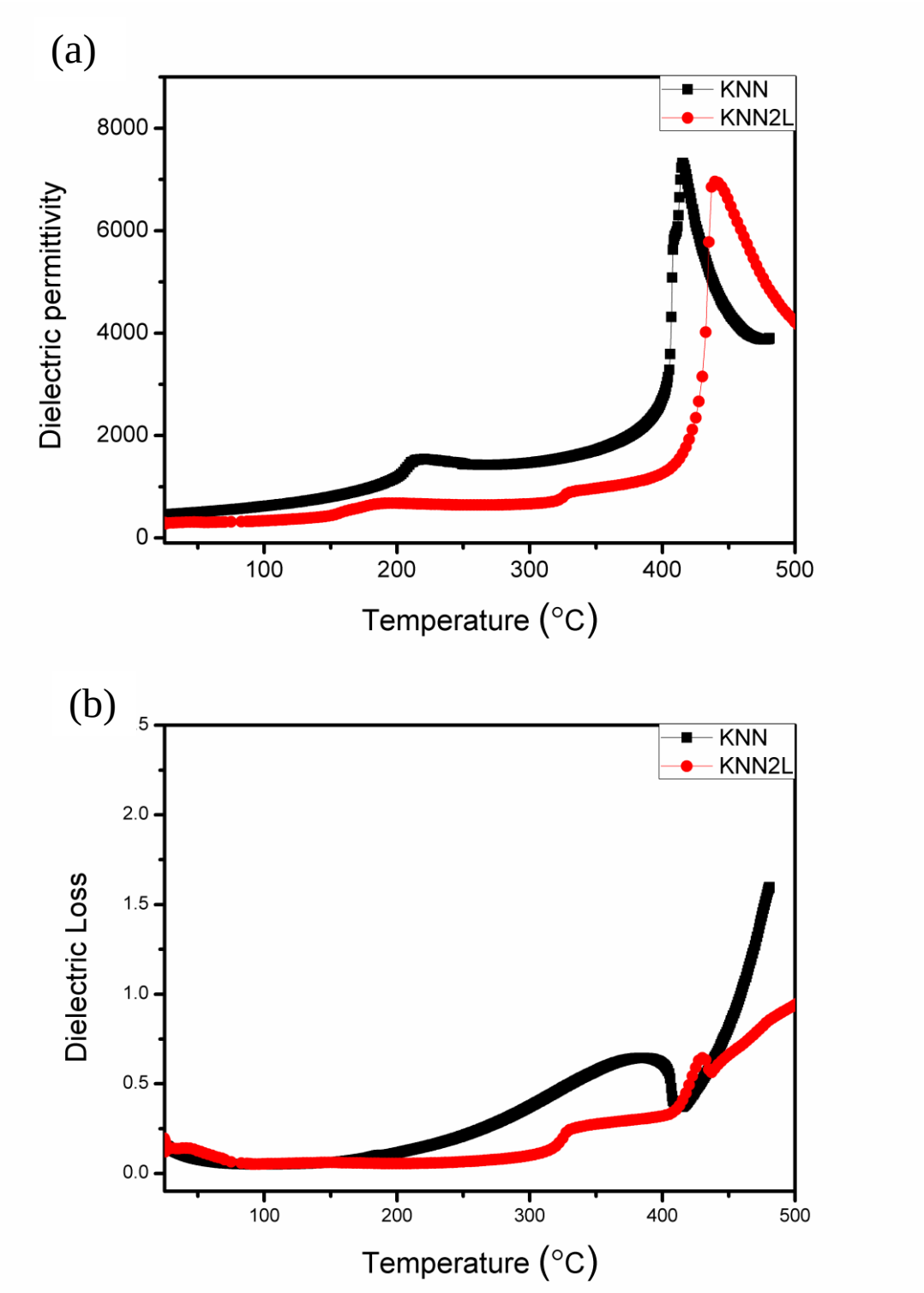

Figure 2: (a) Dielectric permittivity and (b) dielectric loss variation as a function of temperatures of the KNN and KNNL ceramics.

Complex impedance spectroscopy is a well known technique to describe the electrical properties of polycrystalline electroceramics. Grain and grain boundary contributions to the electrical properties of dielectric materials like conductivity, dielectric constant etc. are better analysed using this technique. The variation of real part of impedance (Z′) with

frequency at various temperatures (from 310 to 470 °C) for KNNL ceramics is shown in Figure 3a. Increase in ac conduction (σ_{ac}) in the sample was observed due to the decrease in the magnitude of Z' with rise in temperature. This increase in ac conduction with temperature may be due to the contribution of defects like oxygen vacancies. Generally, the contribution due to oxygen vacancies is more prominent in perovskite structures at elevated temperatures. Higher value of Z' at lower frequency at all temperatures and merging of Z' at higher frequency (> 10 kHz) for all temperatures, is an indication of the presence of space charge polarization [28, 29]. At higher temperature the impedance seems to be independent of frequency and temperature as pointed out by the merging of Z' at higher frequencies.

The variation of imaginary part of impedance (Z'') with frequency for KNNL at different temperature is shown in Figure 3b. Z'' value increases initially, attain a peak (Z''_{max}) and then decreases with frequency at all measured temperatures. Furthermore, Z''_{max} peaks shifts and broadening was observed at higher frequencies with increasing temperature. The appearance of temperature dependent peaks (Z''_{max}) at a characteristic frequency ($\omega_{max}=2\pi f_{max}$) indicates the presence of relaxation process, which is temperature dependent [30]. These relaxation processes may be due to the presence of immobile species at low temperature and defects which became mobile at high temperature. Z'' versus frequency curves were found to merge at a specific frequency in the higher frequency region, which might be due to the reduction in space charge polarization at higher frequency.

Figure 3c shows complex impedance spectrum (Nyquist plot, a plot between the real (Z') and imaginary (Z'') of complex impedance Z*) of KNNL ceramic. The impedance data from room temperature up to about 310 °C is not illustrated in the figure as they just showed a straight line with large slope signifying the high insulating behaviour. However, as the temperature increased the slope decreased and found to curve towards the major (Z') axis forming clear semicircular arcs. The radius of curvature was found to decrease with increasing temperature, which indicates the increase in conductivity of the sample with temperature. Generally, existence of a single semicircular arc represents only one contribution e.g. grain interior (bulk) property of the material. However, in the present case, the spectrum comprises of suppressed semicircular arcs indicating two different contributions from the grain interior (bulk) and grain boundary. The observed semicircular arcs have their centers lying off the real (Z') axis which is an indicative of non-Debye type relaxation with a distribution of relaxation times instead of a single relaxation process. In general, the relaxation time for grain boundary region is much larger than that for the grains and, therefore, its response relaxes at lower frequencies. Thus, the low frequency arc in the Nyquist plot corresponds to the grain boundary effects and the smaller high frequency arc to the grain/bulk effect of the material. The resistance value for the grain (R_g) at a given temperature is equal to the intercept of the corresponding semicircle with the x-axis. The capacitance (C_g) related to a grain can be calculated using R_g and the frequency of maxima (f_{max}) of the semicircle from the equation [18]

$$\omega\tau = 2\pi f_{max} RC = 1$$

The fitted values of R_g, C_g, R_{gb}, C_{gb} for the sample at various temperatures are enlisted in Table 1. Fitting was done by using an equivalent electric circuit consisting of two resistances in series and capacitance in parallel by using Z-view software (Ver. 3.2c, Scribner Associates, Inc) and values of resistance and capacitance for the bulk and grain boundary were calculated. Fitting the data showed a good agreement with the experimental data. In all cases, it was observed that R_{gb} is higher than R_b.

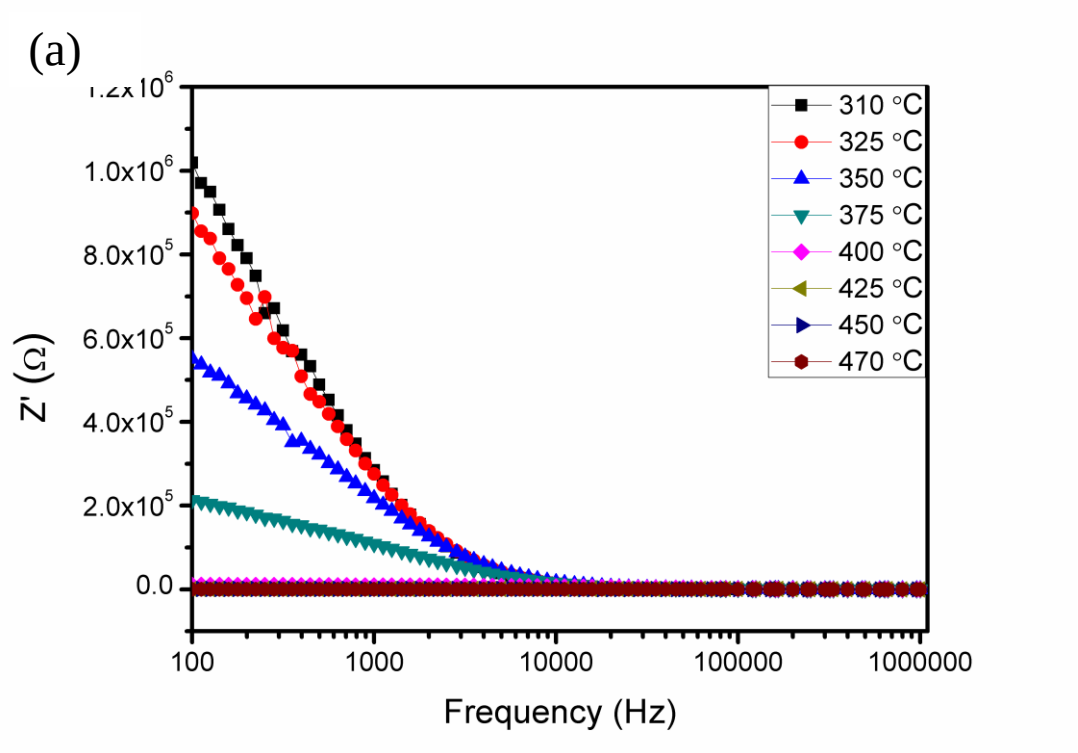
(a)
Z' (Ω)
1.2x10^6
1.0x10^6
8.0x10^5
6.0x10^5
4.0x10^5
2.0x10^5
0.0
100
1000
10000
100000
1000000
Frequency (Hz)
310 °C
325 °C
350 °C
375 °C
400 °C
425 °C
450 °C
470 °C

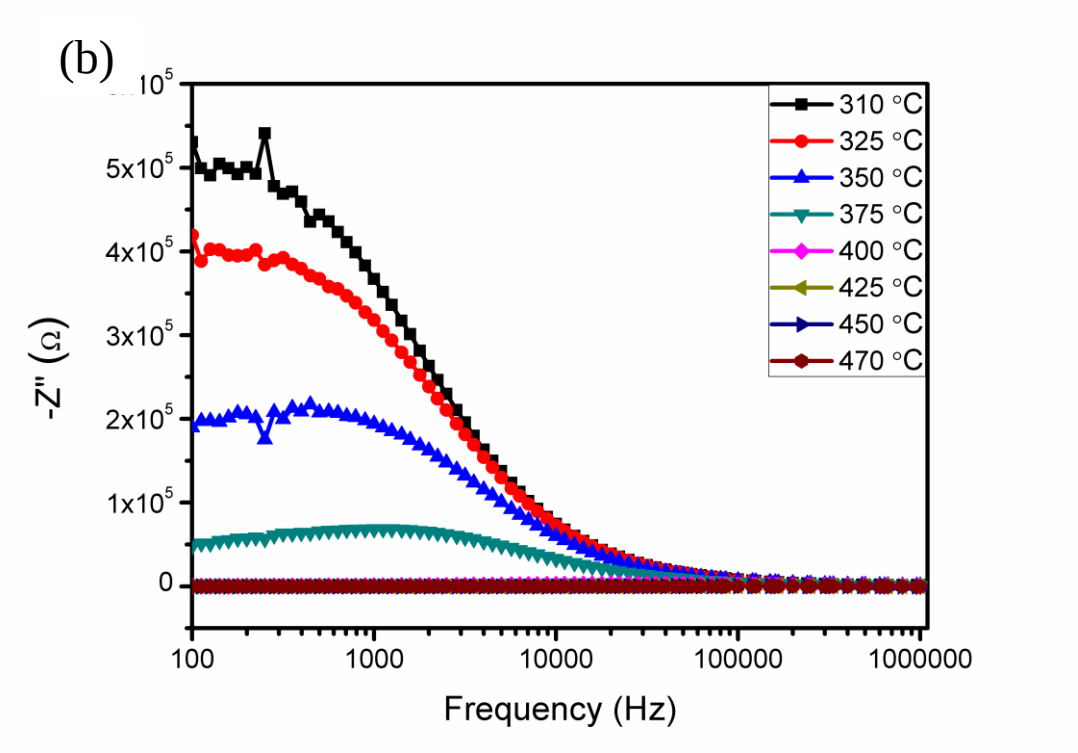
(b)
-Z'' (Ω)
6x10^5
5x10^5
4x10^5
3x10^5
2x10^5
1x10^5
0
100
1000
10000
100000
1000000
Frequency (Hz)
310 °C
325 °C
350 °C
375 °C
400 °C
425 °C
450 °C
470 °C

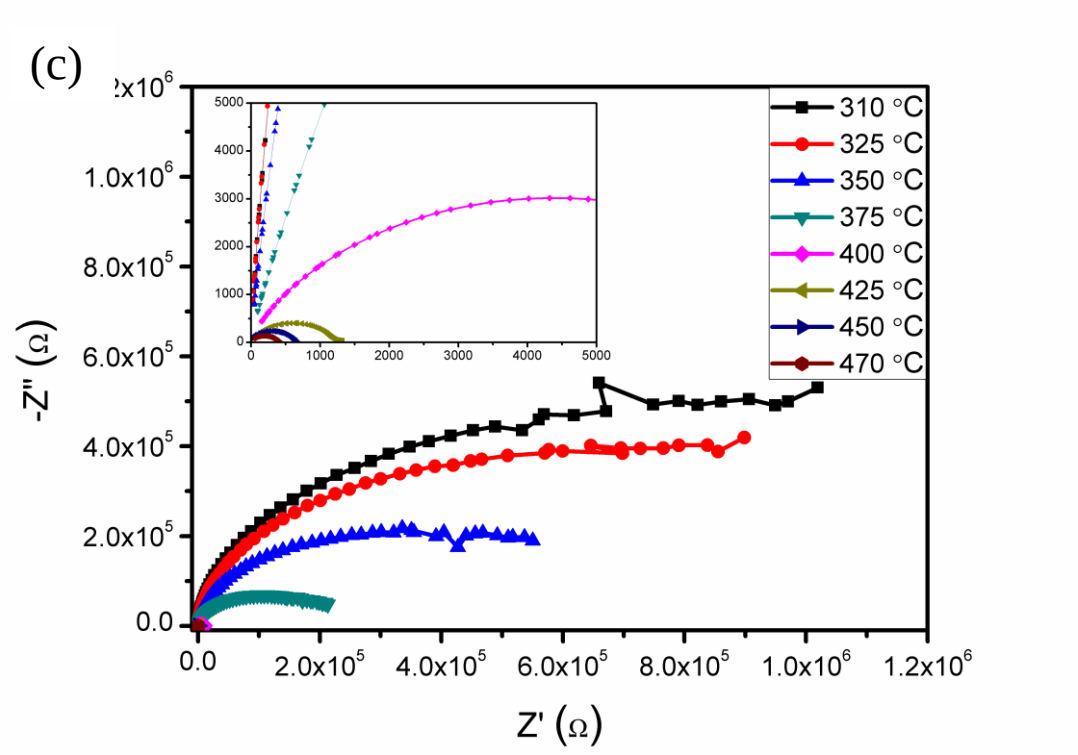

Figure 3: (a, b) Real and imaginary part of impedance variation with frequency and (c) Nyquist plots between imaginary and real part of impedance at different temperatures for KNNL sample.

Table 1. Resistance and capacitance of bulk and grain boundaries of KNNL ceramics after fitting.

T °C	R_b Ohm	C_b F	R_{gb} Ohm	C_{gb} F
310	326330	2.65E-10	959490	7.68E-10
325	266630	2.69E-10	772770	7.77E-10
350	154310	2.93E-10	422000	9.43E-10
375	27658	4.39E-10	159260	8.96E-10
400	1504	4.84E-10	7192	1.18E-09
425	475.4	5.09E-10	739.6	2.62E-09
450	218.5	1.97E-09	427.7	6.30E-09
470	174.3	1.45E-09	223.7	7.70E-09

Complex modulus formalism is an alternative approach to analyze the electrical response of the materials. The modulus formalism sometimes is more useful to distinguish the grain / grain boundary effect as compared to the complex impedance plots [31]. The electric modulus (M) is expressed as:

$$M^* = M' + jM'' = j\times 2\pi f C_o Z^* = j\times 2\pi f C_o(Z' + jZ'')$$

where $C_o = \varepsilon_o A/d$ is the geometrical capacitance, A is the electrode area and d is the distance between the electrodes. Hence, the impedance data have been re-plotted in the modulus formalism as shown in Figure 4 at the same temperatures as has been shown for the complex

impedance plots. Figure 4a shows two semicircular arcs in the complex modulus plots with a small semicircle at high frequency and a large semi-circular arc in the low frequency region at all the temperatures. The modulus spectrum shows a marked change in the shape with rise in temperature suggesting a probable change in the capacitance value as a function of temperature. Figure 4b shows the complex impedance plot along with the fitting as per the equivalent circuit as explained in the previous section. Two contributions are more obvious in the modulus formalism.

Figure 4c shows the variation of real part of electric modulus with frequency at higher temperatures between 310 °C to 470 °C for KNNL ceramics. It is characterized by a low value of M′ in the low frequency region followed by a continuous dispersion with increase in frequency. It was found that M′ values saturated to a maximum in the high frequency region for all temperatures as shown in Figure 4c. This may be contributed to the short range mobility of charge carriers in the studied temperature range.

Figure 4d shows the plot of imaginary part of dielectric modulus at different temperatures for KNNL ceramics. The peak was found to shift towards higher frequency side with increasing temperature. Physically, the peak in the imaginary part of the electric modulus defines the regions where the carrier can move at long distances (left to the peak) or confinement (right to the peak). Also, a peak in the M″ imaginary part indicates a dielectric relaxation process in the solid, and the frequency to the maximum indicates the mean relaxation time of this process. As can be seen, the imaginary part of the electric modulus exhibits a very well defined peak.

(a)

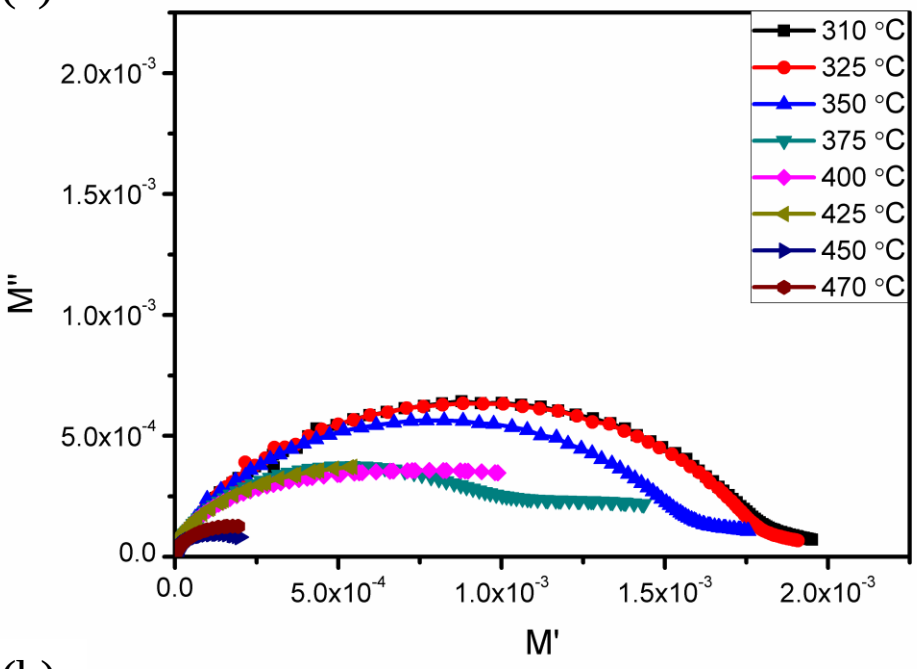

(b)

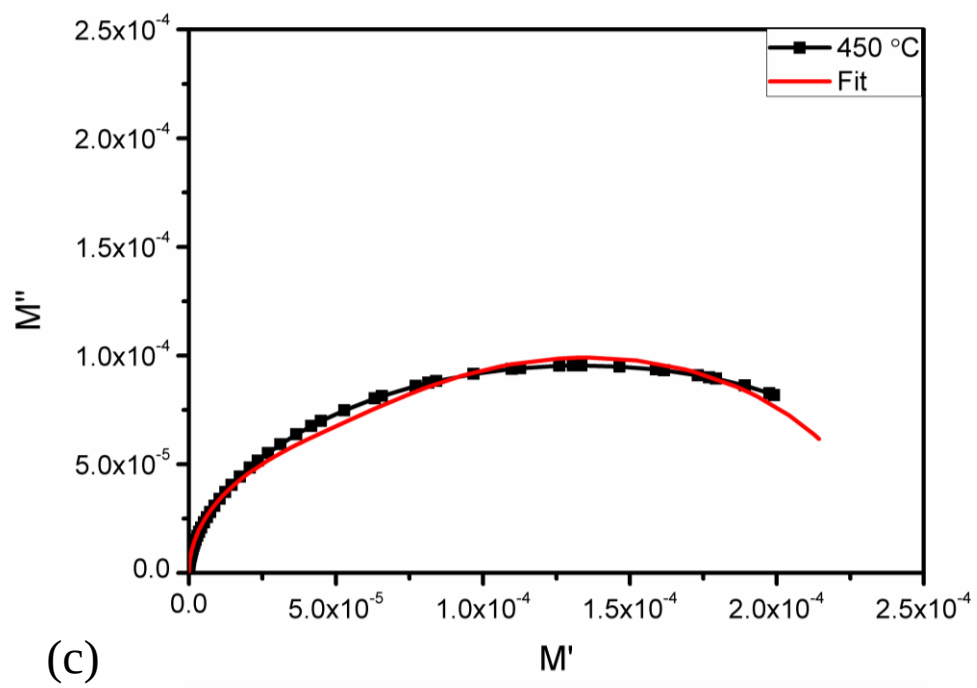
450 °C
Fit
M''
M'
2.5x10-4
2.0x10-4
1.5x10-4
1.0x10-4
5.0x10-5
0.0
0.0
5.0x10-5
1.0x10-4
1.5x10-4
2.0x10-4
2.5x10-4

(c)

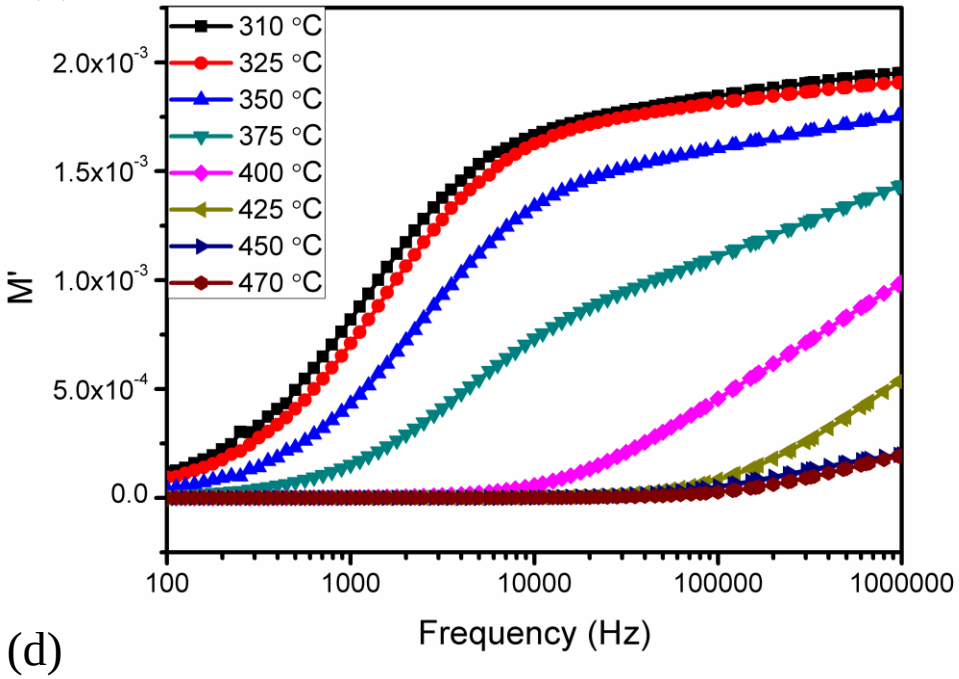
310 °C
325 °C
350 °C
375 °C
400 °C
425 °C
450 °C
470 °C
M'
Frequency (Hz)
2.0x10-3
1.5x10-3
1.0x10-3
5.0x10-4
0.0
100
1000
10000
100000
1000000

(d)

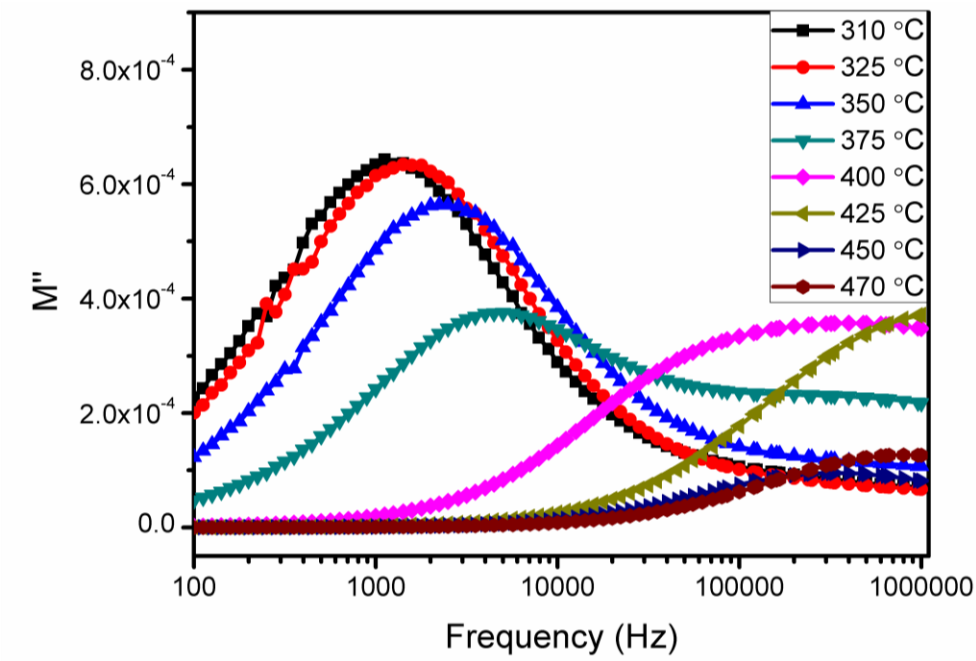

Figure 4. Graphs, (a) between real and imaginary part of modulus, (b) along with the fitting done by Z-view at 450 °C, (c) variation of the real and (d) imaginary parts of modulus as a function of frequency at different temperatures for KNNL sample, respectively.

Figure 5 shows the variation of ac conductivity (σ_{ac}) with temperature (310 - 470 °C) at 10 kHz. The σ_{ac} can be expressed in terms of the permittivity (ε_r) and the dissipation factor (tan δ) as:

$$\sigma_{ac} = \omega \varepsilon_r \varepsilon_o \tan \delta$$

where ω ($=2\pi f$) is the angular frequency and ε_o is free-space permittivity. As observed, conductivity increases with increasing temperature. Moreover, the variation exhibits a change of slope with increasing temperatures. In order to clarify the conduction mechanisms responsible for the observed behaviour, the values of the activation energy for conduction (σ_{ac}) were calculated assuming an Arrhenius behaviour [18]:

$$\sigma_{ac} = \sigma_0 \left(-\frac{E_a}{K_b T}\right)$$

where σ_0 stands for the pre-exponential term, k_B for Bolzmann constant, T for absolute temperature and E_a for the activation energy of conduction. The activation energy values calculated is 0.41 eV. It has been reported that for single-ionized oxygen vacancies the activation energies fall in the range 0.3 - 0.5 eV while for doubly-ionized oxygen vacancies it is 0.6 - 1.2 eV [32, 33]. Considering this, the results obtained for the studied sample suggest that the conduction process could be related to single-ionized state of the oxygen vacancies.

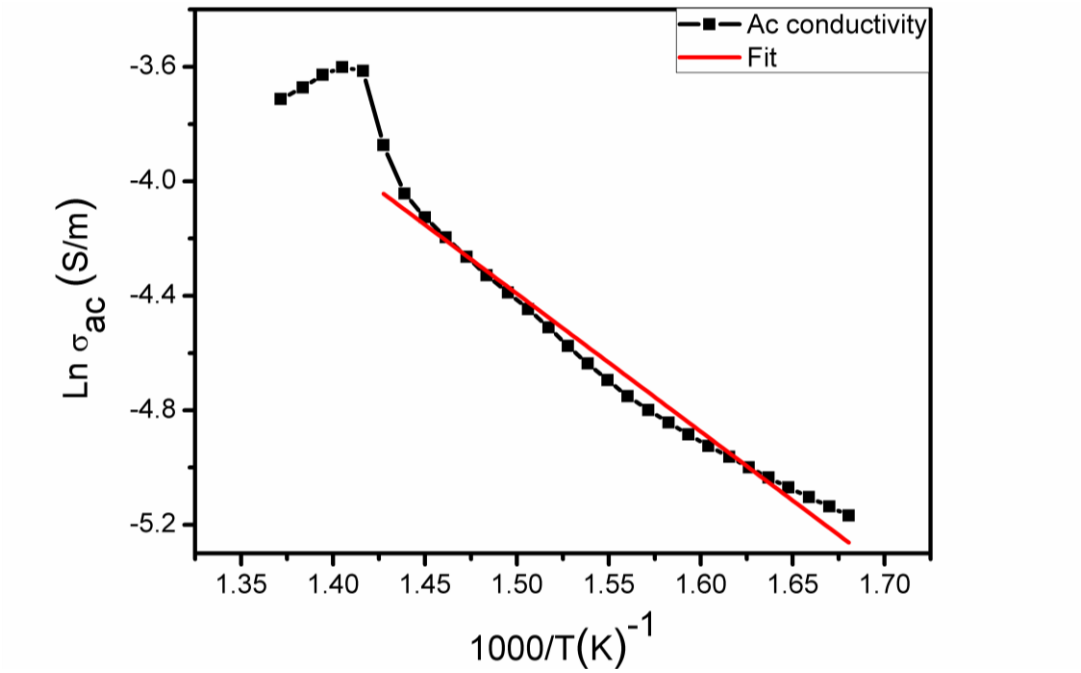

Figure 5. Variation of ac conductivity versus inverse of temperature for KNNL samples.

4. Conclusions

KNN and Li doped polycrystalline KNN ceramic samples have been synthesized by solid-state reaction method.

- The dielectric studies performed on the single- phase KNNL sample revealed anomalies around 439 ºC and 155 ºC.
- Two peaks in the dielectric permittivity were correlated to the phase transition from cubic to tetragonal (T_C) and tetragonal to monoclinic ($T \rightarrow M$) upon cooling, respectively.
- Complex impedance spectroscopic measurements reveal that the electrical relaxation process was temperature dependent and of non-Debye type.
- AC conductivity and values of activation energy of conduction (0.41eV) showed that conductivity in KNNL samples was mainly due to the single-ionized oxygen vacancies.

References

1. Park, S.-E. and Shrout, T.R., Applied Physics Letters. 82(4), 1804 (1997)
2. Jaeger, R.E. and Egerton, L., J. Am. Ceram. Soc. 45, 209 (1962)
3. Shirane, G., Newnham, R., and Pepensky, R., Physical Review. 96(3), 581 (1954)
4. Jaffe, B., Cook, W.R., and Jaffe, H., *Piezoelectric ceramics*. Vol. 3. 1971, London: Acadamic Press.
5. Jaeger, R.E. and Egerton, L., Journal of the American Ceramic Society. 45(5), 209 (1962)
6. Tellier, J., et al., Solid State Sciences. 11(2), 320 (2009)
7. Ge, W., et al., Journal of Applied Physics. 111(10), 103503 (2012)
8. Saito, Y., et al., Nature. 432(7013), 84 (2004)

9. Guo, Y.P., Kakimoto, K., and Ohsato, H., Applied Physics Letters. 85(18), 4121 (2004)
10. Zang, G.-Z., et al., Applied Physics Letters. 88(21) (2006)
11. Zhang, S., et al., Journal of Applied Physics. 100(10), 104108 (2006)
12. Chang, Y.F., et al., Applied Physics Letters. 90(23), 232905 (2007)
13. Akdogan, E.K., et al., Applied Physics Letters. 92(11), 112908 (2008)
14. Skidmore, T.A., Comyn, T.P., and Milne, S.J., Applied Physics Letters. 94(22), 222902 (2009)
15. Dai, Y.J., Zhang, X.W., and Zhou, G.Y., Applied Physics Letters. 90(26), 262903 (2007)
16. Webber, K.G., Zuo, R., and Lynch, C.S., Acta Materialia. 56(6), 1219 (2008)
17. Kobor, D., et al., Journal of Physics D-Applied Physics. 40(9), 2920 (2007)
18. Macdonald, J.R. and Johnson, W.B., *Impedance Spectroscopy: Theory, Experiment, and Applications*. Second ed2005: John Wiley & Sons, Inc.
19. Sinclair, D.C. and West, A.R., Journal of Applied Physics. 66(8), 3850 (1989)
20. Suchanicz, J., Materials Science and Engineering B-Solid State Materials for Advanced Technology. 55(1-2), 114 (1998)
21. Sinclair, D.C. and West, A.R., Physical Review B. 39(18), 13486 (1989)
22. Macdonald, J.R. and Johnson, W.B., *Fundamentals of impedance spectroscopy*, in *Impedance Spectroscopy*2005, John Wiley & Sons, Inc. p. 1.
23. Rafiq, M.A., Costa, M.E., and Vilarinho, P.M., Science of Advanced Materials. Accepted (2013)
24. Klein, N., et al., Journal of Applied Physics. 102(1), 014112 (2007)
25. Lin, D.M., et al., Smart Materials & Structures. 17(3), 035002 (2008)
26. Matsubara, M., et al., Japanese Journal of Applied Physics Part 1-Regular Papers Short Notes & Review Papers. 44(1A), 258 (2005)
27. Matsubara, M., et al., Japanese Journal of Applied Physics. 44(8), 6136 (2005)
28. Suchanicz, J., Materials Science and Engineering: B. 55(1–2), 114 (1998)
29. Sen, S. and Choudhary, R.N.P., Materials Chemistry and Physics. 87(2–3), 256 (2004)
30. Jonscher, A.K., Nature. 267(5613), 673 (1977)
31. Srivastava, A., Garg, A., and Morrison, F.D., Journal of Applied Physics. 105(5), 054103 (2009)
32. Pelaiz-Barranco, A., et al., Journal of Physics D-Applied Physics. 41(21), 215503 (2008)
33. Raymond, O., et al., Journal of Applied Physics. 97(8), 084107 (2005)